Applied Catalysis B: Environmental 162 (2015) 412–419

Contents lists available at ScienceDirect

Applied Catalysis B: Environmental

journal homepage: www.elsevier.com/locate/apcatb

Simultaneous catalytic oxidation of carbon monoxide, hydrocarbons and soot with Ce–Zr–Nd mixed oxides in simulated diesel exhaust conditions

Leandro P. dos Santos Xavier, Verónica Rico-Pérez, Ana M. Hernández-Giménez, Dolores Lozano-Castelló, Agustín Bueno-López*

Department of Inorganic Chemistry, University of Alicante, Ap. 99, E-03080 Alicante, Spain

ARTICLE INFO

Article history:
Received 21 May 2014
Received in revised form 3 July 2014
Accepted 5 July 2014
Available online 11 July 2014

Keywords:
Diesel soot
Carbon monoxide
Hydrocarbons
Ceria–zirconia catalyst
Neodymium–ceria catalyst

ABSTRACT

$Ce_{0.73-x}Zr_{0.27}Nd_xO_2$ mixed oxides ($x \leq 0.3$) were prepared, characterized by XRD, Raman spectroscopy, N_2 adsorption isotherms and H_2-TPR, and tested for simultaneous CO, propylene, benzene and soot oxidation in a gas mixture containing O_2, NO_x, H_2O, CO_2, CO, propylene (model aliphatic hydrocarbon) and benzene (model aromatic hydrocarbon) that simulates a diesel exhaust. Ce–Zr mixed oxide doping with a low atomic fraction of neodymium ($0.01 \leq x \leq 0.09$) promotes the creation of oxygen vacancies, has a minor effect in the BET specific surface areas of the oxides, increases the surface ceria reducibility and has a positive effect in the catalytic activity. On the contrary, higher neodymium atomic fractions ($x = 0.2$ and 0.3) promote sintering, with a drastic decrease of the BET specific surface area, surface reducibility and catalytic activity. The $Ce_{0.73-x}Zr_{0.27}Nd_xO_2$ catalysts with $x \leq 0.09$ are able to accelerate simultaneously soot, propylene and benzene combustion, and as a general trend, the catalytic behavior of $Ce_{0.73}Zr_{0.27}O_2$ is improved by low atomic fraction neodymium doping ($0.01 \leq x \leq 0.09$). These $Ce_{0.73-x}Zr_{0.27}Nd_xO_2$ mixed oxides with $0.01 \leq x \leq 0.09$ are also able to accelerate CO oxidation in a certain extent, but there is a net production of CO during soot combustion because the oxidation capacity of these oxides is not high enough to oxidize all CO released as soot combustion product.

1. Introduction

Cerium-based oxides are part of the active phases used in three way catalysts (TWC) for gas pollution control in gasoline vehicles [1–4]. Cerium oxides improve noble metals dispersion and stabilization, store and release oxygen buffering the fluctuations of the O_2 concentration in the gas mixture and catalyze (together with noble metals) some reactions like CO and hydrocarbons oxidation.

Cerium oxide-based catalysts have been also proposed for soot combustion in diesel vehicles, where the gas exhaust is highly oxidizing [5–9]. Diesel engines also emit CO and hydrocarbons, but in much lower concentration than gasoline engines [10–13]. Usually, a platinum-containing diesel oxidation catalyst (DOC) is used in diesel vehicles for simultaneous CO, hydrocarbons and NO oxidation. The NO_2 produced, which is much more oxidizing than NO and O_2, starts the combustion of soot collected downstream in a diesel particulate filter (DPF).

Noble metal-free catalysts are being investigated for soot combustion in diesel exhausts in order to lower the cost of the after-treatment devices. Ceria-based oxides are promising candidates, and the role of O_2 and NO_x in the ceria-catalyzed combustion of soot is well understood. One of the ceria-catalyzed soot-combustion mechanisms consists of the oxidation of NO to NO_2 (as described for platinum-containing DOC), and other consists of the production of active oxygen by oxygen exchange between the ceria-based catalyst and the oxygen-containing gas molecules, mainly O_2. Depending on the ceria catalyst features and on the reaction conditions (temperature, gas composition, etc.) either both mechanisms progress synergically together or one of them prevails.

Platinum catalysts are much more active for NO oxidation to NO_2 than ceria catalysts, but the latters are able to approach the activity of platinum for soot combustion if the active oxygen mechanism gets involved. The main handicap of the active oxygen mechanism is that the contact between soot and ceria catalyst particles must allow the active oxygen species to be transferred from catalyst to soot, otherwise they recombine to each other and yield O_2 [14]. Therefore, ceria catalysts must be impregnated into the DPF instead

* Corresponding author. Tel.: +34 600948665; fax: +34 965903454.
E-mail address: agus@ua.es (A. Bueno-López).

http://dx.doi.org/10.1016/j.apcatb.2014.07.013
0926-3373/

of being loaded in a DOC located upstream the DPF, as usually done with platinum.

The substitution of the Pt-DOC + DPF soot removal device by a ceria-DPF configuration seems promising, but it must be analyzed whether ceria-catalysts are able to remove simultaneously soot, hydrocarbons and CO, as platinum catalyst does, or if further improvements are required.

We have recently analyzed the effect of H_2O, CO_2 and SO_2 in the catalytic activity for soot combustion of $Ce_{0.73}Zr_{0.27}O_2$ and $Ce_{0.64}Zr_{0.27}Nd_{0.09}O_2$ in simulated diesel exhaust conditions, concluding that all these three gases lower the activity of both catalysts and that the inhibiting effect follows the trend $SO_2 \ggg H_2O > CO_2$ [15]. The poisoning effect of SO_2 was already reported by other authors [16–19], but less attention was paid in the literature to the effect of H_2O and CO_2. In situ DRIFTS experiments showed that CO_2, H_2O and SO_2 compete with NO_x for the adsorption sites on the catalysts' surface [15]. CO_2 and H_2O partially hinder the catalytic oxidation of NO to NO_2 while SO_2 chemisorption inhibits almost all the activity due to sulfate formation. The catalytic activity for soot combustion of $Ce_{0.64}Zr_{0.27}Nd_{0.09}O_2$ was equal or higher to that of $Ce_{0.73}Zr_{0.27}O_2$ in the presence of NO_x, O_2, H_2O and/or CO_2, because Nd^{3+} doping promotes the participation of the active oxygen mechanism, which seems to resists the presence of H_2O and CO_2 better than the NO_2-assisted soot combustion mechanism [15]. For this reason, the $Ce_{0.64}Zr_{0.27}Nd_{0.09}O_2$ mixed oxide was identified as a potential catalyst with practical relevance for diesel vehicles running with sulfur-free fuel, since it maintained significant activity for soot combustion even in the presence of H_2O and CO_2.

As far as we know, the simultaneous ceria-catalyzed combustion of soot, CO, and hydrocarbons has not been studied and reported in the literature, and this is one of the goals of the current study. In addition, the positive effect of Nd^{3+} doping in the catalytic activity the Ce–Zr mixed oxide for soot combustion, which was first reported in [20], has lead us to focus the current study to ternary Ce–Zr–Nd mixed oxides. A series of $Ce_{0.73-x}Zr_{0.27}Nd_xO_2$ mixed oxides were prepared with different neodymium content, and were characterized and tested for the simultaneous oxidation of CO and hydrocarbons, both in the absence and presence of soot. A complex gas mixture that mimics a diesel engine exhaust containing NO_x, O_2, H_2O, CO_2, CO, propylene and benzene was used. Propylene and benzene were selected as model aliphatic and aromatic hydrocarbons, respectively.

2. Experimental details

2.1. Catalysts preparation

Six $Ce_{0.73-x}Zr_{0.27}Nd_xO_2$ mixed oxides were prepared, with $x = 0$, 0.01, 0.05, 0.09, 0.2 and 0.3. Formally, the stoichiometric coefficient of oxygen in the neodymium-containing catalysts should be lower than 2, since the tetravalent cation "$Ce^{4+\prime}$" is replaced by a trivalent one (Nd^{3+}). However, the subscript 2 has been maintained in the nomenclature for the sake of simplicity.

The required amounts of $Ce(NO_3)_3{\cdot}6H_2O$ (Sigma Aldrich, 99%), $Nd(NO_3)_3{\cdot}6H_2O$ (Aldrich, 99.9%) and/or $ZrO(NO_3)_2{\cdot}xH_2O$ (Fluka, $x \approx 6$) were dissolved in water and an ammonia solution was dropped to keep the pH at about 9, leading to the precipitation of the cations. After filtering, the precipitates were firstly dried at 110 °C in air overnight and then calcined in air at 800 °C for 90 min to ensure thermal stability and practical meaning.

The synthesis method and the amount of zirconium on the mixed oxides were selected based on our previous studies on soot combustion, where catalysts with different Ce–Zr ratios were prepared by different methods [21,22].

2.2. Catalysts characterization

X-ray diffractograms of the catalysts were recorded in a Rigaku Miniflex II diffractometer, using CuK_α radiation ($\lambda = 0.15418$ nm). The diffractograms were recorded between 10° and 80° (2θ) with a step of 0.025°.

Raman spectra were recorded in a Bruker RFS 100/S Fourier Transform Raman Spectrometer with a variable power Nd–YAg laser source (1064 nm). The laser beam was focused on the sample in a 180° backscattering configuration and 128 scans at 100 mW laser power were recorded.

The BET specific surface area of the oxides was determined by physical adsorption of N_2 at −196 °C in an automatic volumetric system (Autosorb-6, Quantachrome). The samples were outgassed at 150 °C for 4 h before the N_2 adsorption measurements.

Temperature programed reduction (H_2-TPR) experiments were carried out with 15 mg of fresh mixed oxide, which were pretreated in situ at 500 °C for 1 h in a 35 mL/min flow of 5 vol.% O_2 in He. Once cold, the flow gas was switched to 35 mL/min of 5 vol.% H_2 in Ar and the temperature was increased at 10 °C/min up to 1050 °C.

2.3. Catalytic tests

Catalytic tests were performed at atmospheric pressure in a cylindrical reactor coupled simultaneously to a HP 6890 gas chromatograph equipped with a TCD and two columns (Porapak Q, for CO_2 and Molecular Sieve 13×, for O_2, N_2 and CO) and a Pfeiffer Vacuum mass spectrometer (model OmniStar) to monitor NO, propylene, NO_2 and benzene concentrations following the m/z = 30, 39, 46 and 78 signals, respectively. The total flow rate was 100 mL/min (GHSV = 42,000 h^{-1}) and the gas composition was 300 ppm CO/120 ppm propylene/3% CO_2/180 ppm benzene/1000 ppm NO_x (~0 ppm NO_2)/5%O_2/2%H_2O and He as balance gas. Gas flow controllers were used to feed the required amount of each individual gas, and the O_2 flow was bubbled in water at 72 °C before mixing with the remaining flows to add steam into the gas mixture. This complex composition simulates a real diesel engine exhaust and allows evaluating the simultaneous catalytic oxidation of CO, propylene, benzene and soot in quite realistic conditions.

Catalytic tests were performed with and without soot. Experiments performed without soot consisted of the simultaneous CO, propylene and benzene catalytic oxidation studied at selected temperatures from room temperature up to 550 °C. 100 mg of each mixed oxide catalyst was used for these experiments, which were diluted with 300 mg of SiC to avoid pressure drop and favor heat transfer. The experiments were extended until steady-state at each temperature, typically for 30 min.

Experiments were also performed with 100 mg of catalyst mixed with 25 mg of soot and 300 mg of SiC. Soot and catalyst were mixed with a spatula in the so-called loose contact conditions to simulate the contact in a real DPF filter [23]. The model soot used was a carbon black supplied by Evonik–Degussa GmbH (Printex U). The soot-catalyst-SiC mixture was heated at 530 °C in 13 mL/min He. Then, the inert gas was replaced by the reactive gas mixture and the gas composition was monitored as a function of time.

Propylene and benzene conversions were determined following the m/z 39 and 78 signals, respectively, by mass spectrometry and CO conversions were determined from gas chromatography measurements. The conversions of CO, propylene and benzene were calculated as follows:

$$\text{Conversion}\,(\%) = 100 \times \left(\frac{[\text{pollutant}]_{\text{in}} - [\text{pollutant}]_{\text{out}}}{[\text{pollutant}]_{\text{in}}} \right)$$

where $[pollutant]_{in}$ and $[pollutant]_{out}$ are the inlet and outlet concentrations, respectively, of each gas pollutant (CO, propylene and benzene).

Soot conversion was determined from CO_2 and CO evolved (both followed by gas chromatography) after subtracting the stoichiometric amounts of CO_2 corresponding to the propylene, benzene and CO conversions assuming oxidation of these gases to CO_2 and H_2O.

3. Results and discussion

3.1. Catalysts characterization

Fig. 1 shows the X-ray diffractograms of the $Ce_{0.73-x}Zr_{0.27}Nd_xO_2$ catalysts. The main peaks observed in this figure correspond to the typical cubic structure of ceria. A shoulder is also distinguished in all diffractograms at high angles of the (1 1 1) cubic peak, which evidences the formation of a tetragonal segregated phase. The cations sublattice is similar in the cubic and tetragonal structures, corresponding to a face-centered cubic (fcc) framework with cations placed in the corners and faces center of a cubic unit cell. The difference between the cubic and tetragonal frameworks is the position of the oxygen anions. Oxygen anions are placed in the octahedral positions in the cubic structure while they are out these positions (four above and four below the equilibrium positions) in the tetrahedral structure [24–27]. Tetragonalization of the cubic structure of pure ceria typically occurs upon partial substitution of the Ce^{4+} cations (0.097 nm) by smaller Zr^{4+} cations (0.084 nm), because the oxygen anions are displaced from the octahedral position to relax the tensions created by different size cations. The segregation of a cerium-rich cubic structure and a zirconium-rich tetragonal structure was already observed for $Ce_{0.73}Zr_{0.27}O_2$ and $Ce_{0.64}Zr_{0.27}Nd_{0.09}O_2$ oxides [20], and this conclusion is now extended to a wider range of neodymium atomic fractions.

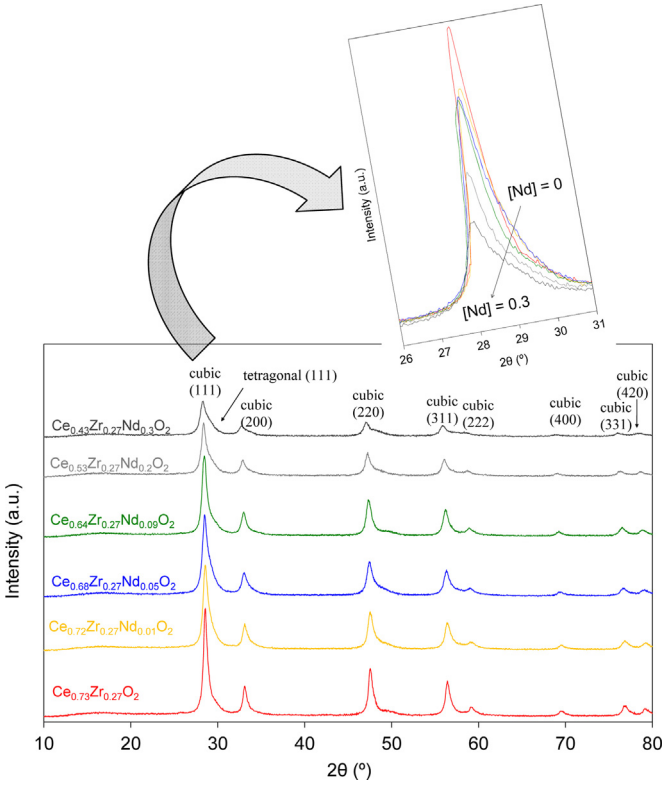

Fig. 1. X-ray diffractograms of the $Ce_{0.73-x}Zr_{0.27}Nd_xO_2$ oxides.

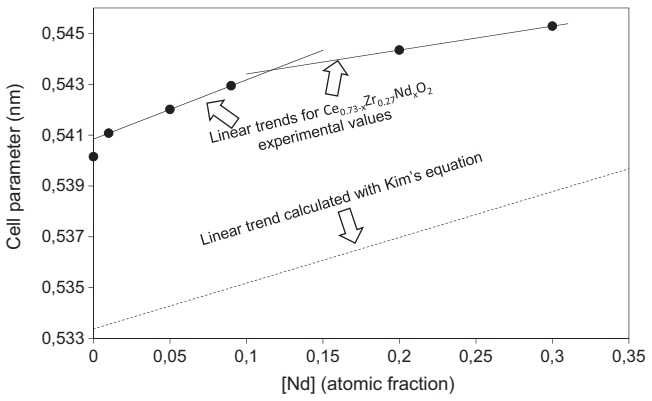

Fig. 2. Cell parameter of the $Ce_{0.73-x}Zr_{0.27}Nd_xO_2$ oxides determined from X-ray diffractograms.

The XRD peaks positions, intensity and broadening strongly depends on the neodymium atomic fraction (see inset in Fig. 1), because the introduction of large trivalent Nd^{3+} cations (0.112 nm) distorts the lattices. The crystal sizes have not been estimated from XRD because the presence of the segregated tetragonal zirconium-rich phase hinders the proper estimation of the cubic peaks broadening. It is also difficult to quantify the amount of dopants actually loaded into the ceria lattice for ternary Ce–Zr–Nd mixed oxides, because the cell expansion produced by Nd^{3+} doping faces the cell contraction produced by Zr^{4+}doping. However, some information can be obtained from the cell parameters determined from the (1 1 1) peak position, which can be properly determined for all oxides in spite of the tetragonal peak shoulder. The experimentally measured cell parameters are plotted in Fig. 2 together with the theoretical values estimated for pure Ce–Zr–Nd solid solutions using the Kim's equation [28,29]:

$$\text{Cell parameter (nm)} = 0.5411 - 0.000286 \cdot m_{Zr} + 0.00018 \cdot m_{Nd}$$

where m_{Zr} and m_{Nd} are the atomic % of zirconium and neodymium in the Ce–Zr–Nd solid solution, respectively. This empirical equation is based on the Vegard's rule, which predicts a linear relationship between the lattice parameter and the concentration of dopants in a solid solution.

The experimental cell parameters of all samples are well above the theoretical trend predicted for a pure solid solution, in agreement with the segregation of part of the zirconium in a tetragonal phase. For $Ce_{0.73-x}Zr_{0.27}Nd_xO_2$ mixed oxides with $x \leq 0.09$, the slope of the linear trend followed by the experimental values with regard to the neodymium concentration is quite similar to that predicted by the Kim's equation, suggesting that the insertion of neodymium cations into the cubic lattice of ceria is quite good and better to that of zirconium. This slope decreases for higher neodymium concentrations, which suggests that Nd^{3+} loading into the parent ceria lattice becomes more difficult for 0.2 and 0.3 neodymium atomic fractions.

The better insertion of neodymium cations into the ceria lattice in comparison with those of zirconium can be explained taking into account the charge of the cations precursors used for the preparation of the mixed oxides, being +3 for cerium and neodymium while +4 for zirconium. The coprecipitation of cations upon ammonia adding is much more homogeneous for cations with the same charge and similar size (0.114 nm for Ce^{3+} and 0.112 nm for Nd^{3+}), because their acid strength is similar, than for cations of different charge and size. That is why, in the current study, cerium and neodymium formed better solid solutions than cerium and zirconium. It must be taken into account that cerium precursors with both +3 and +4 charges exist, while not for zirconium and neodymium which are only available in the +4 and +3 oxidation

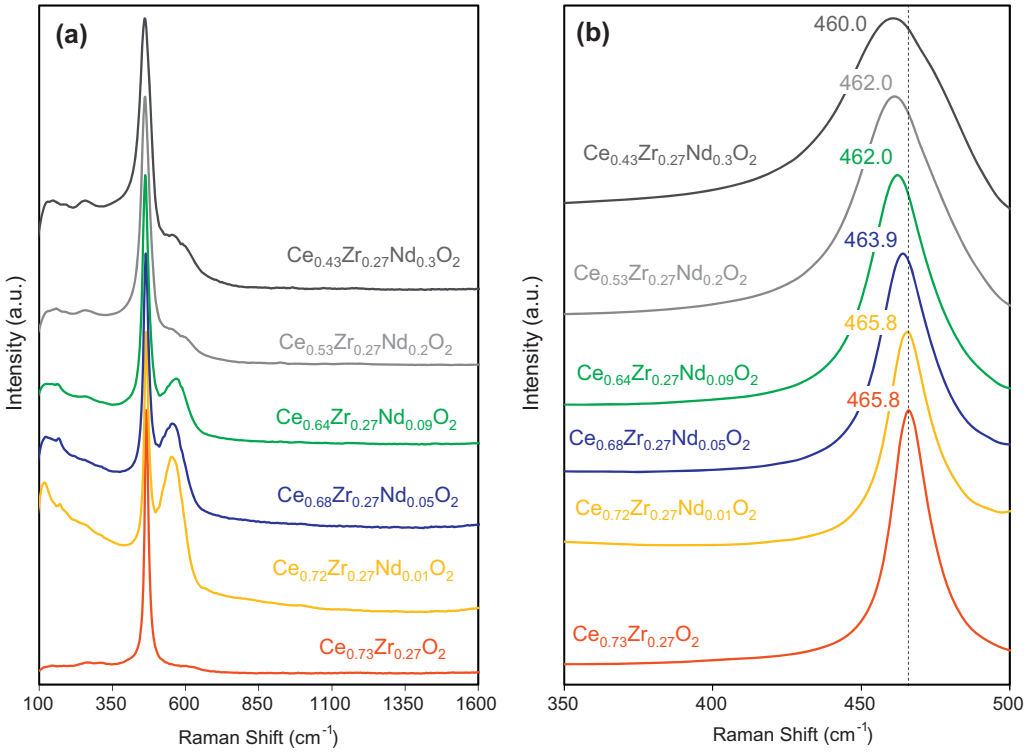

Fig. 3. Raman spectra of the $Ce_{0.73-x}Zr_{0.27}Nd_xO_2$ oxides. (a) General view of the 100–1600 cm^{-1} range and (b) detail of the F_{2g} ceria peak centered at 460–465.8 cm^{-1}.

states, respectively. Our choice for the current study was to use a Ce^{3+} precursor because the study is focused on the effect of neodymium loading, but in a previous article the effect of the cerium precursor in the features of binary Ce–Zr oxides was discussed in detail [30]. It is known that much better insertion of Zr^{4+} into the ceria framework would be obtained with the selection of a Ce^{4+} precursor, but this would be hindered Nd^{3+} doping.

Raman spectra included in Fig. 3 also provided information about the structure of the oxides, and supported some conclusions of the XRD analysis. All spectra show a Raman band centered at 460–465.8 cm^{-1}, which is assigned to the F_{2g} mode of the fluorite-type cubic structure of cerium oxides [31,32]. The presence of low-intensity bands in the range 120–300 cm^{-1} has been related to the tetragonal shift of the oxygen anions from the ideal octahedral positions that occupy in the fluorite cubic structure [33,34], which typically occurs upon zirconium insertion into the CeO_2 lattice. The displacement of the F_{2g} band position toward low Raman shifts by increasing the neodymium atomic fraction (see Fig. 3b) is an evidence of the introduction of large Nd^{3+} cations into the parent cubic structure of ceria. The creation of oxygen vacancies is related to the shoulder at 620 cm^{-1} [35], and the intensity of this shoulder suggests that the number of vacancies increases significantly for low neodymium atomic fractions ($x \leq 0.09$) but it is not so relevant for higher neodymium content ($x = 0.2$ and 0.3). This is consistent with the cell parameter trend determined by XRD (see Fig. 2), which suggested that the neodymium insertion becomes worse for mixed oxides with 0.2 and 0.3 neodymium atomic fractions.

The BET specific surface areas also showed important differences among $Ce_{0.73-x}Zr_{0.27}Nd_xO_2$ mixed oxides. The values plotted in Fig. 4 show that the BET specific surface areas ranged from 0 to 31 m^2/g. These low values were expected considering that the oxides were sintered at 800 °C to provide practical meaning to the study. The BET surface area of the neodymium-free Ce–Zr mixed oxide (26 m^2/g) is in line with typical values previously obtained for similar materials with the same thermal history [20,21], and slightly higher areas were obtained for $Ce_{0.73-x}Zr_{0.27}Nd_xO_2$ oxides with $0.01 \leq x \leq 0.09$. However, higher neodymium atomic fractions lead to an important sintering of the mixed oxides with a drastic decrease of the BET surface area down to 8 and 0 m^2/g for $x = 0.2$ and 0.3, respectively. The existence of an optimum dopant loading has been already reported for some other mixed oxides. Zhang et al. [36,37] studied La^{3+}-doped TiO_2 oxides and reported that the optimum lanthanum atomic fraction was 1% in order to avoid the phase transformation of titania. This amount of lanthanum was estimated to correspond to a monolayer of surface cations, and further increase of the dopant concentration above the monolayer coverage induced the segregation of lanthanum oxide and titanium oxide. This argument could also be applied to our $Ce_{0.73-x}Zr_{0.27}Nd_xO_2$ mixed oxides, that is, low neodymium atomic fractions ($x \leq 0.09$) seem to slightly stabilize the mixed oxide, while higher neodymium contents have the opposite effect, in spite of evidences of segregated neodymium phases were neither obtained by XRD nor by Raman spectroscopy.

The characterization of the mixed oxides was also carried out by Temperature Programed Reduction with H_2, and the obtained

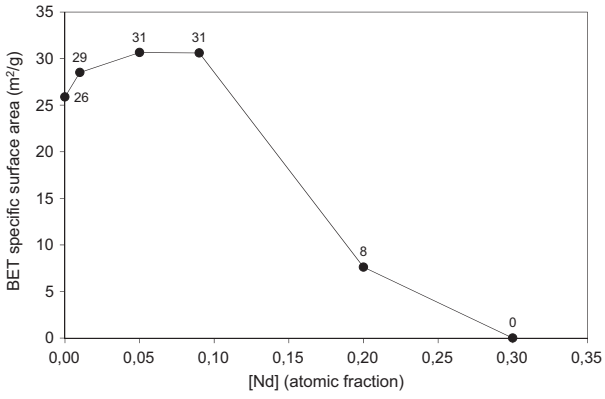

Fig. 4. BET specific surface area of the $Ce_{0.73-x}Zr_{0.27}Nd_xO_2$ oxides.

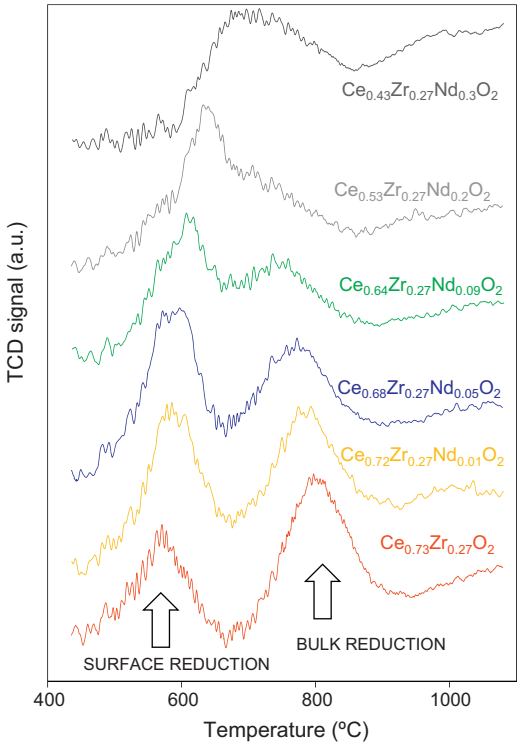

Fig. 5. TCD profiles obtained in temperature programed reductions with H_2 of the $Ce_{0.73-x}Zr_{0.27}Nd_xO_2$ oxides.

profiles were drawn in Fig. 5. Note that the only reducible cations in the $Ce_{0.73-x}Zr_{0.27}Nd_xO_2$ mixed oxides are Ce^{4+}, while both Zr^{4+} and Nd^{3+}, which cannot be reduced in the experimental conditions of the H_2-TPR experiments, modify the redox behavior of the Ce^{4+}/Ce^{3+} couple.

Most H_2-TPR profiles consist of a mild-temperature peak around 550 °C, which is attributed to surface reduction of the mixed oxides, and a high-temperature peak assigned to bulk reduction. The formation of two well-defined reduction peaks in most of the mixed oxides studied occurs because there is an energetic restriction for the bulk oxygen to move until the particles surface, and high temperature is required to promote such oxygen mobility.

The surface and bulk reduction-peak temperatures are plotted in Fig. 6 versus the neodymium atomic fraction. The neodymium loading affected both the surface and bulk reduction. The bulk reduction peak shifted toward lower temperature with the neodymium content increase (see Fig. 6), and the surface and bulk reduction peaks even merge for the highest neodymium-content mixed oxides (see

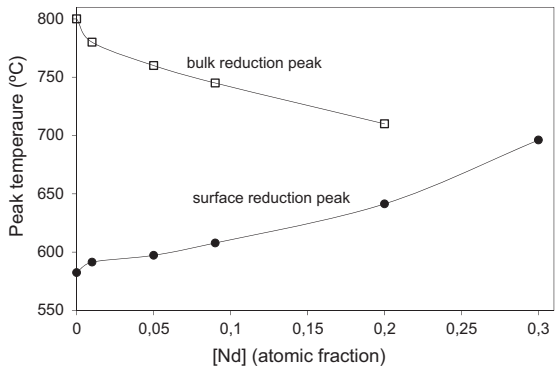

Fig. 6. Temperature of the surface and bulk reduction peaks obtained in H_2-TPR experiments with the $Ce_{0.73-x}Zr_{0.27}Nd_xO_2$ oxides.

Fig. 5). This occurs because the introduction of large trivalent Nd^{3+} cations into the parent ceria–zirconia framework improves the mobility of oxygen into the lattice, and only 0.01 neodymium atomic fraction is enough to shift significantly the bulk reduction peak. The effect of neodymium on surface reduction was the opposite, and the surface reduction-peak temperature was delayed toward higher temperatures as the neodymium atomic fraction was increased. This delay was small for $Ce_{0.73-x}Zr_{0.27}Nd_xO_2$ mixed oxides with $x \leq 0.09$, but became much more relevant for $x = 0.2$ and 0.3, which is consistent with the very low surface area of these two mixed oxides (8 and 0 m^2/g). However, the area under the surface reduction peak (see Fig. 5) increased for $Ce_{0.72}Zr_{0.27}Nd_{0.01}O_2$ and $Ce_{0.68}Zr_{0.27}Nd_{0.05}O_2$ with respect to $Ce_{0.73}Zr_{0.27}O_2$, that is, few neodymium increased the amount of surface Ce^{4+} reduced.

As a summary, the characterization results have shown that the $Ce_{0.73-x}Zr_{0.27}Nd_xO_2$ mixed oxides prepared consist of two segregated ceria-rich and zirconium rich phases with proper neodymium doping for $x \leq 0.09$. This is a consequence of the preparation method used, where Ce^{3+}, Nd^{3+} and Zr^{4+} cations were precipitated. Doping the Ce–Zr mixed oxides with low atomic fractions of neodymium promoted the creation of oxygen vacancies, had a minor effect on the BET specific surface area of the oxides, increased the amount of surface Ce^{4+} reduced and, as it will be discussed in the coming section, had a positive effect on the catalytic activity. On the contrary, higher neodymium atomic fractions ($x = 0.2$ and 0.3) had a negative effect on the mixed oxides features because promote sintering, with a drastic decrease of the BET specific surface area and of the surface reducibility. These worst features of $Ce_{0.53}Zr_{0.27}Nd_{0.2}O_2$ and $Ce_{0.43}Zr_{0.27}Nd_{0.3}O_2$ are also evidenced in the catalytic behavior in the next section.

3.2. Catalytic tests

Catalytic tests were performed with the $Ce_{0.73-x}Zr_{0.27}Nd_xO_2$ oxides in the absence and presence of soot under a complex gas mixture with O_2, NO_x, H_2O, CO_2, CO, propylene (model aliphatic hydrocarbon) and benzene (model aromatic hydrocarbon). The consumption of NO_x was negligible in all cases, and the discussion is focused on the removal of the remaining pollutants (CO, hydrocarbons and soot).

Fig. 7 shows the conversion percentages and conversion rates of propylene, benzene and CO obtained in steady state at different temperatures. The catalytic activities for the conversion of these three pollutants of the $Ce_{0.73-x}Zr_{0.27}Nd_xO_2$ mixed oxides with $x \leq 0.09$ were significantly higher than those of the mixed oxides with higher neodymium content. This behavior is consistent with the drastic decrease of the BET surface area and surface reducibility of $Ce_{0.53}Zr_{0.27}Nd_{0.2}O_2$ and $Ce_{0.43}Zr_{0.27}Nd_{0.3}O_2$ with regard to the $Ce_{0.73-x}Zr_{0.27}Nd_xO_2$ mixed oxides with $x \leq 0.09$.

CO conversion started above 300 °C for all catalysts and increased smoothly with temperature achieving 30% conversion at 550 °C for $Ce_{0.73-x}Zr_{0.27}Nd_xO_2$ mixed oxides with $x \leq 0.09$. Propylene and benzene conversions needed temperatures above 350 and 400 °C, respectively, to occur in measurable extents in the experiment performed with $Ce_{0.73}Zr_{0.27}O_2$, which is the most active catalyst at low temperature among those prepared in this study. The onset temperatures for propylene and benzene conversion were slightly higher for the $Ce_{0.73-x}Zr_{0.27}Nd_xO_2$ mixed oxides with $x = 0.01$, 0.05 and 0.09 than for $Ce_{0.73}Zr_{0.27}O_2$. However, the conversions rose faster with temperature for these neodymium-containing mixed oxides and they were more active than $Ce_{0.73}Zr_{0.27}O_2$ at the highest temperatures tested. This change of the reaction order of neodymium-free and neodymium-containing Ce–Zr mixed oxides at different temperatures could be related with the surface reducibility of these oxides, as studied by

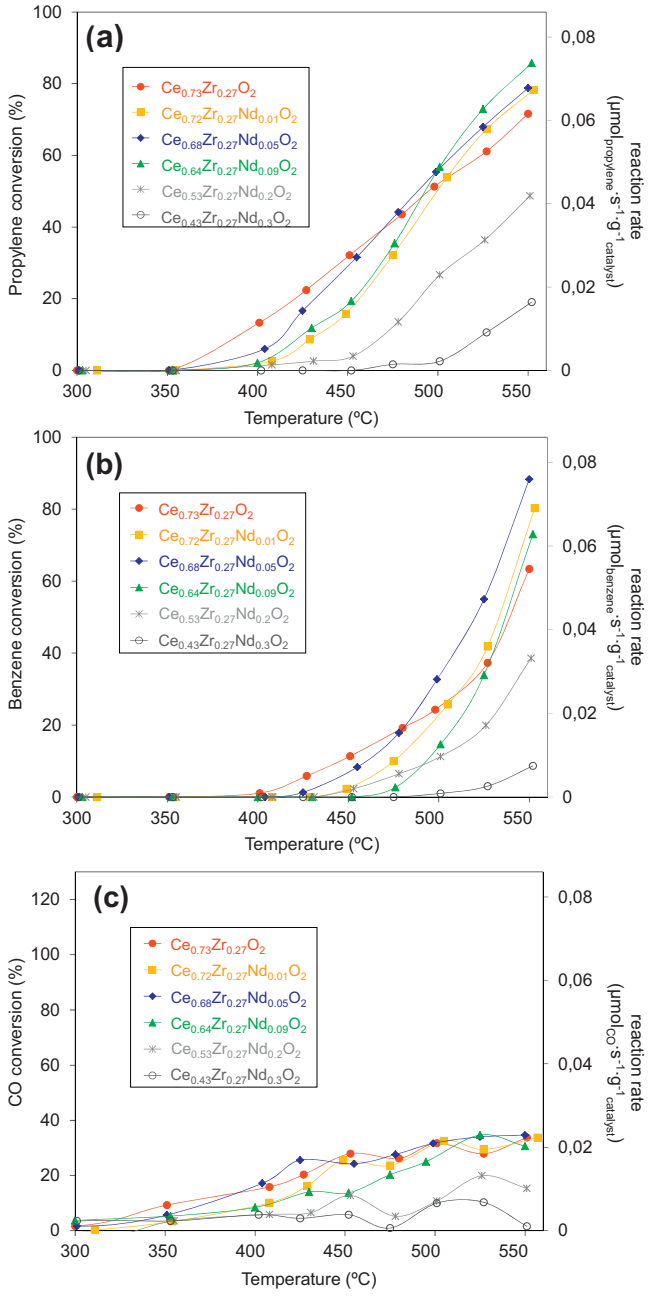

Fig. 7. Catalytic tests performed at different temperatures with the $Ce_{0.73-x}Zr_{0.27}Nd_xO_2$ oxides in the absence of soot. (a) Propylene, (b) benzene and (c) CO.

H_2-TPR (see Figs. 5 and 6). The temperature for maximum signal in the surface reduction peak was the lowest for $Ce_{0.73}Zr_{0.27}O_2$ (Fig. 6), and the onset temperatures for propylene and benzene conversions were also the lowest for this catalyst (Fig. 7a and b). The surface reduction peak temperature was slightly higher for the $Ce_{0.73-x}Zr_{0.27}Nd_xO_2$ mixed oxides with $x = 0.01$, 0.05 and 0.09 than for $Ce_{0.73}Zr_{0.27}O_2$ (Fig. 6), and so does the onset propylene and benzene conversion temperatures (Fig. 7a and b, respectively), but once the temperature was high enough for these reactions to occur the conversions rose faster for the neodymium-containing catalysts. This could be tentatively attributed to the improved oxygen mobility upon neodymium doping, which would restore faster the oxygen balance on the catalyst surface after consumption in propylene and benzene oxidation. This agreement between the surface reduction behavior observed by H_2-TPR experiments and

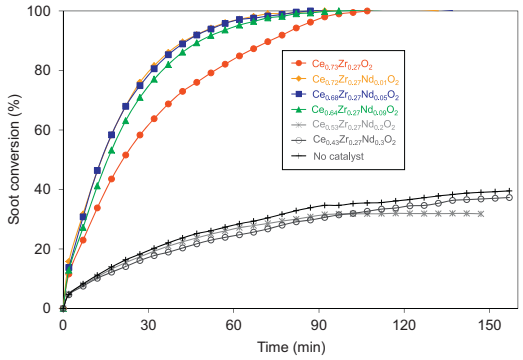

Fig. 8. Soot conversion in catalytic tests performed at 530 °C with the $Ce_{0.73-x}Zr_{0.27}Nd_xO_2$ oxides mixed in loose contact with soot.

the catalytic combustion of propylene and benzene suggest that redox mechanisms are taking place, as typically occurs in oxidation reactions catalyzed by cerium-based oxides [3,38].

Soot combustion experiments were also performed at 530 °C under the complex gas mixture with O_2, NO_x, H_2O, CO_2, CO, propylene and benzene that simulates a diesel exhaust, and the soot conversion profiles were plotted in Fig. 8 as a function of time. The most active soot combustion $Ce_{0.73-x}Zr_{0.27}Nd_xO_2$ catalysts are those with $x = 0.01$, 0.05 and 0.09. These low neodymium atomic fractions improved the $Ce_{0.73}Zr_{0.27}O_2$ catalytic activity, while the improvement in activity for soot combustion is null for the mixed oxides with higher neodymium atomic fraction ($Ce_{0.53}Zr_{0.27}Nd_{0.2}O_2$ and $Ce_{0.43}Zr_{0.27}Nd_{0.3}O_2$). This behavior is in line with the previously discussed conversions of CO, propylene and benzene obtained in experiments performed without soot (Fig. 7). The improved catalytic activity for soot combustion of the Ce–Zr mixed oxide catalyst by 0.09 atomic fraction neodymium doping was already reported [20], but the current study analyzes the effect of neodymium in a wider range of concentrations and in a more complex gas mixture.

The removal of propylene, benzene and CO was analyzed during soot combustion, and the conversion profiles were plotted in Fig. 9 with regard to soot conversion. The propylene conversion percentage was around 90% for the $Ce_{0.73-x}Zr_{0.27}Nd_xO_2$ mixed oxides with $x \leq 0.09$, while remained much lower for $Ce_{0.53}Zr_{0.27}Nd_{0.2}O_2$ and $Ce_{0.43}Zr_{0.27}Nd_{0.3}O_2$. It was observed that the catalyst temperature (the thermocouple was placed inside the reactor facing the catalytic bed) increased few degrees (~3–5 °C) during the exothermal soot combustion, and this leads to think that the local increase of temperature could be higher in local hot spots at the soot-catalyst particles interface. This could explain why propylene conversions obtained in the presence of soot (Fig. 9) were slightly higher than those obtained in the absence of soot (Fig. 7).

The conversions of benzene during soot combustion were lower than those of propylene (Fig. 9), in accordance with the behavior in the absence of soot (Fig. 7), and the $Ce_{0.73-x}Zr_{0.27}Nd_xO_2$ mixed oxides with $x \leq 0.09$ were more active than $Ce_{0.53}Zr_{0.27}Nd_{0.2}O_2$ and $Ce_{0.43}Zr_{0.27}Nd_{0.3}O_2$, which showed almost null activity.

Finally, the CO conversion profiles obtained in catalytic combustion experiments performed with soot (Fig. 9c) were very different to those obtained without soot (Fig. 7c). Actually, most CO conversion values were negative during soot combustion, that is, CO was actually emitted in experiments with soot instead of being depleted. The $Ce_{0.73-x}Zr_{0.27}Nd_xO_2$ mixed oxides with $x = 0.01$, 0.05 and 0.09 reached positive CO conversion values, once soot was consumed (see inset in Fig. 9c), what means that there is a net production of CO during soot combustion because the catalytic CO oxidation rates seem to be lower than the CO emission rate by soot combustion. It was estimated in a previous study that 75% of soot

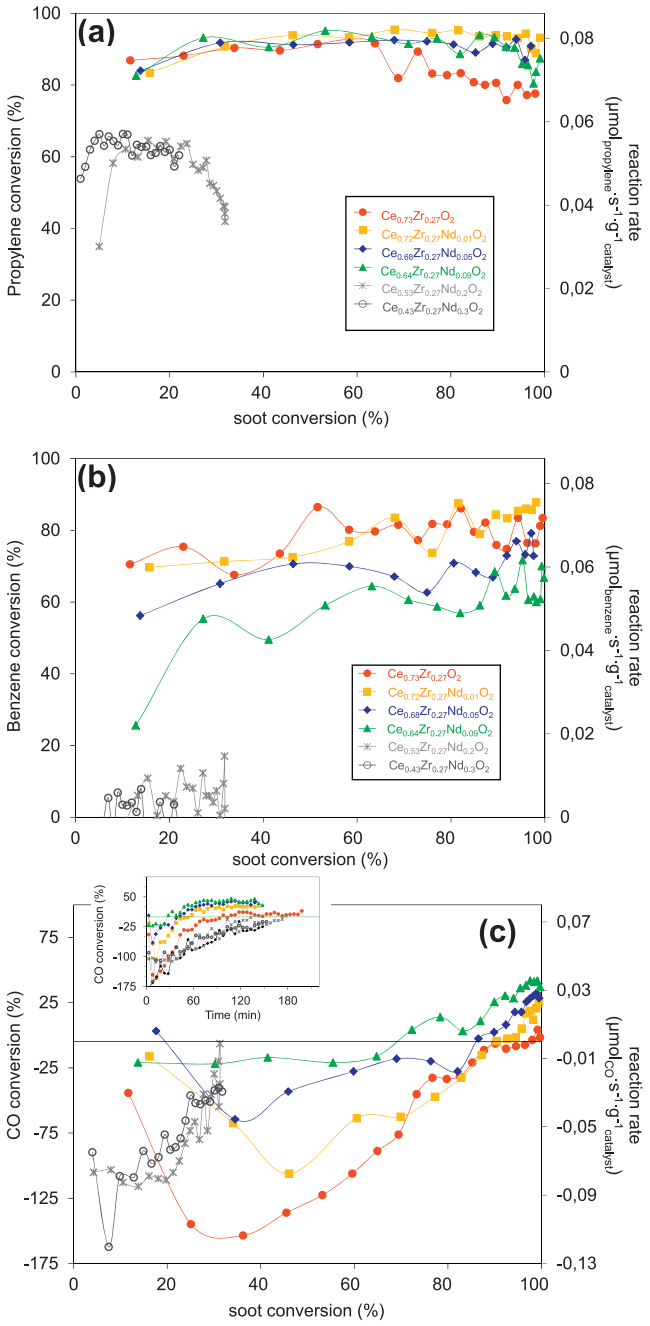

Fig. 9. Catalytic tests performed at 530 °C with the $Ce_{0.73-x}Zr_{0.27}Nd_xO_2$ oxides mixed in loose contact with soot. (a) Propylene, (b) benzene and (c) CO.

was oxidized to CO_2 in a $Ce_{0.64}Zr_{0.27}Nd_{0.09}O_2$-catalysed combustion of soot, while the remaining 25% yielded CO. The emission of CO as soot combustion product could be positive if a deNO_x device (by selective catalytic reduction – SRC or NO_x storage and reduction – NSR) is going to be located downstream the ceria-DPF, because CO would contribute to NO_x reduction and would save reductant. On the contrary, if the ceria-DPF is the last device in the after-treatment system actions must be taken to avoid CO release, for instance, including into the DPF a transition metal like copper with high CO oxidation capacity.

As a summary, the catalytic tests performed in the current study evidenced that some $Ce_{0.73-x}Zr_{0.27}Nd_xO_2$ catalysts were able to accelerate simultaneously soot, propylene and benzene combustion. As a general trend, the catalytic behavior of $Ce_{0.73}Zr_{0.27}O_2$ was improved by low atomic fraction neodymium doping ($0.01 \leq x \leq 0.09$), while a very negative effect was obtained for higher loading ($x = 0.2$ and 0.3). The $Ce_{0.73-x}Zr_{0.27}Nd_xO_2$ mixed oxides were also able to accelerate CO oxidation in a certain extent, but there was a net production of CO during soot combustion because the oxidation capacity of these oxides was not high enough to oxidize all CO released as soot combustion product.

4. Conclusions

$Ce_{0.73-x}Zr_{0.27}Nd_xO_2$ mixed oxides ($x = 0$, 0.01, 0.05, 0.09, 0.2 and 0.3) were prepared, characterized, and tested for simultaneous CO, propylene, benzene and soot combustion in simulated diesel exhaust conditions, and the following conclusions can be summarized:

- The $Ce_{0.73-x}Zr_{0.27}Nd_xO_2$ mixed oxides consisted of two segregated ceria-rich and zirconium-rich phases with proper neodymium doping for atomic fractions of $x \leq 0.09$. This was a consequence of the preparation method used, where Ce^{3+}, Nd^{3+} and Zr^{4+} cations were precipitated.
- Doping of the Ce–Zr mixed oxides with low neodymium atomic fractions ($x \leq 0.09$) promoted the creation of oxygen vacancies, had a minor effect on the BET specific surface area of the oxides, increased the amount of surface Ce^{4+} reduced and had a positive effect on the catalytic activity. On the contrary, higher neodymium atomic fractions ($x = 0.2$ and 0.3) had a negative effect on the mixed oxides features because promoted sintering, with a drastic decrease of the BET specific surface area, surface reducibility, and catalytic activity.
- The $Ce_{0.73-x}Zr_{0.27}Nd_xO_2$ catalysts with $x \leq 0.09$ were able to accelerate simultaneously soot, propylene and benzene oxidation. As a general trend, the catalytic behavior of $Ce_{0.73}Zr_{0.27}O_2$ was improved by low atomic fraction neodymium doping ($0.01 \leq x \leq 0.09$), while a very negative effect was obtained for higher loading ($x = 0.2$ and 0.3).
- The $Ce_{0.73-x}Zr_{0.27}Nd_xO_2$ mixed oxides were also able to accelerate CO oxidation in a certain extent, but there was a net production of CO during soot combustion because the oxidation capacity of these oxides was not high enough to oxidize all CO released as soot combustion product.

Acknowledgments

The authors thank the financial support of CNPq – National Counsel of Technological and Scientific Development (Brazil), of the Spanish Ministry of Economy and Competitiveness (Project CTQ2012-30703) and of the UE (FEDER funding).

References

[1] G. Kim, Ind. Eng. Chem. Prod. Res. Dev. 21 (1982) 267–274.
[2] A.F. Diwell, R.R. Rajaram, H.A. Shaw, T.J. Truex, Stud. Surf. Sci. Catal. 71 (1991) 139–152.
[3] A. Trovarelli, C. De Leitenburg, M. Boaro, G. Dolcetti, Catal. Today 50 (1999) 353–367.
[4] H.S. Gandhi, G.W. Graham, R.W. McCabe, J. Catal. 216 (2003) 433–442.
[5] E. Aneggi, C. de Leitenburg, G. Dolcetti, A. Trovarelli, Catal. Today 114 (2006) 40–47.
[6] A.M. Hernández-Giménez, D. Lozano Castelló, A. Bueno-López, Chem. Pap. 68 (2014) 1154–1168.
[7] M. Dhakad, T. Mitshuhashi, S. Rayalu, P. Doggali, S. Bakardjiva, J. Subrt, D. Fino, H. Haneda, N. Labhsetwar, Catal. Today 132 (2008) 188–193.
[8] M. Machida, Y. Murata, K. Kishikawa, D. Zhang, K. Ikeue, Chem. Mater. 20 (2008) 4489–4494.
[9] A. Bueno-López, Appl. Catal. B 146 (2014) 1–11.
[10] J.P.A. Neeft, M. Makkee, J.A. Moulijn, Fuel Process. Technol. 47 (1996) 1–69.
[11] B.A.A.L. van Setten, M. Makkee, J.A. Moulijn, Catal. Rev. 43 (2001) 489–564.
[12] M.V. Twigg, Appl. Catal. B 70 (2007) 2–15.
[13] D. Fino, V. Specchia, Powder Technol. 180 (2008) 64–73.

[14] N. Guillén-Hurtado, A. García-García, A. Bueno-López, J. Catal. 299 (2013) 181–187.
[15] A.M. Hernández-Giménez, D. Lozano-Castelló, A. Bueno-López, Appl. Catal. B 148–149 (2014) 406–414.
[16] R. Flouty, E. Abi-Aad, S. Siffert, A. Aboukaıs, Appl. Catal. B 46 (2003) 145–153.
[17] D. Weng, J. Li, X. Wu, F. Lin, Catal. Commun. 9 (2008) 1898–1901.
[18] M.A. Peralta, V.G. Milt, L.M. Cornaglia, C.A. Querini, J. Catal. 242 (2006) 118–130.
[19] K. Tikhomirov, O. Krocher, M. Elsener, A. Wokaun, Appl. Catal. B 64 (2006) 72–78.
[20] A.M. Hernández-Giménez, L.P. dos Santos Xavier, A. Bueno-López, Appl. Catal. A 462–463 (2013) 100–106.
[21] I. Atribak, A. Bueno-Lopez, A. Garcia-Garcia, J. Catal. 259 (2008) 123–132.
[22] I. Atribak, A. Bueno-Lopez, A. Garcia-Garcia, Top. Catal. 52 (2009) 2088–2091.
[23] F. Zhang, C.-H. Chen, R.D. Robinson, I.P. Herman, S.-W. Chan, J. Am. Ceram. Soc. 89 (2006) 1028–1036.
[24] B.A.A.L. van Setten, J.M. Schouten, M. Makkee, J.A. Moulijn, Appl. Catal. B 28 (2000) 253–257.
[25] E. Djurado, P. Bouvier, G.J. Lucazeau, Solid State Chem. 149 (2000) 399–407.
[26] R.C. Garvie, J. Phys. Chem. 82 (1978) 218–224.
[27] A. Gayen, M. Boaro, C. de Leitenburg, J. Llorca, A. Trovarelli, J. Catal. 270 (2010) 285–298.
[28] D.J. Kim, J. Am. Ceram. Soc. 72 (1989) 1415–1421.
[29] M. Mogensen, in: A. Trovarelli (Ed.), Catalysis by Ceria and Related Materials, Imperial College Press, London, 2002, p. 462.
[30] N. Guillén-Hurtado, I. Atribak, A. Bueno-López, A. García-García, J. Mol. Catal. A 323 (2010) 52–58.
[31] A. Mineshige, T. Taji, Y. Muroi, M. Kobune, S. Fujii, N. Nishi, M. Inaba, Z. Ogumi, Solid State Ionics 135 (2000) 481–485.
[32] L.N. Ikryannikova, A.A. Aksenov, G.L. Markayan, G.P. Muravieva, B.G. Kostyuk, A.N. Kharlanov, E.V. Linina, Appl. Catal. A 210 (2001) 225–235.
[33] J. Kaspar, P. Fornasiero, G. Balducci, R. di Monte, N. Hickey, V. Sergo, Inorg. Chim. Acta 349 (2003) 217–226.
[34] S. Letichevsky, C.A. Tellez, R.R. de Avillez, M.I.P. da Silva, M.A. Fraga, L.G. Appel, Appl. Catal. B 58 (2005) 203–210.
[35] A. Martínez-Arias, M. Fernández-García, V. Ballesteros, L.N. Salamanca, J.C. Conesa, C. Otero, J. Soria, Langmuir 15 (1999) 4796–4802.
[36] Y.H. Zhang, H.X. Zhang, Y.X. Xu, Y.G. Wang, J. Solid State Chem. 177 (2004) 3490–3498.
[37] Y.H. Zhang, H.L. Xu, Y.X. Xu, H.X. Zhang, Y.G. Wang, J. Photochem. Photobiol. A 170 (2005) 279–285.
[38] A. Trovarelli, Catal. Rev. Sci. Eng. 38 (1996) 439–520.